Biomaterials Science

Accepted Manuscript

This article can be cited before page numbers have been issued, to do this please use: U. Mangal, T. Kang, J. W. Jung, J. Kim, J. Seo, J. Cha, K. Lee, H. Yu, K. Kim, J. Kim, J. Kwon and S. Choi, *Biomater. Sci.*, 2022, DOI: 10.1039/D2BM01428A.

ROYAL SOCIETY OF CHEMISTRY

rsc.li/biomaterials-science

View Article Online
DOI: 10.1039/D2BM01428A

ARTICLE

Polybetaine-enhanced hybrid ionomer cement shows improved total biological effect with bacterial resistance and cellular stimulation

Received 00th January 20xx,
Accepted 00th January 20xx

DOI: 10.1039/x0xx00000x

Utkarsh Mangal[a, ‡], Tae-Yun Kang[b, ‡], Ju Won Jung[b,c], Ji-Yeong Kim[a,d], Ji-Young Seo[a], Jung-Yul Cha[a], Kee-Joon Lee[a], Hyung-Seog Yu[a], Kwang-Mahn Kim[b], Jin-Man Kim[c, *], Jae-Sung Kwon[b,d, *], and Sung-Hwan Choi [a,d, *]

Hybrid ionomer cements (HICs) are aesthetic polyelectrolyte cements that have been modified with a resin. The setting of HICs occurs by both monomer polymerization and an acid–base reaction. In addition, HICs contain a resin, which is substituted for water. Thus, the competition between the setting reactions and reduced water content inherently limits polysalt formation and, consequently the bioactive interactions. In this study, we explored the effects of polybetaine zwitterionic derivatives (*m*ZMs) on the augmentation of the bioactive response of HICs. The polybetaines were homogenized into an HIC in different proportions (α, β, and γ) at 3% w/v. Following basic characterization, the bioactive response of human dental pulp stem cells (hDPSCs) was evaluated. The augmented release of the principal constituent ions (strontium, silica, and fluoride) from the HIC was observed with the addition of the *m*ZMs. Modification with α-*m*ZM elicited the most favorable bioactive response, namely, increased ion elution, in vitro calcium phosphate precipitation, and excellent biofouling resistance, which deterred the growth of the bridging species of *Veillonella*. Moreover, α-*m*ZM resulted in a significant increase in the hDPSC response, as confirmed by a significant increase ($p < 0.05$) in alizarin red staining. The results of mRNA expression tests, performed using periodically refreshed media, showed increased and early peak expression levels for RUNX2, OCN, and OPN in the case of α-*m*ZM. Based on the results of the in vitro experiments, it can be concluded that modification of HICs with polybetaine α-*m*ZM can augment the overall biological response.

Introduction

Polyelectrolyte cement systems are used extensively in dental therapy. Among the various systems available, ionomeric glass cements (GCs) are unique because of their fluoride release properties and ability to chemically adhere to the tooth surface [1]. However, conventional GCs exhibit limitations such as high brittleness, microleaks at the adhesive interface, and sensitivity to water. These issues were overcome by second-generation GCs through hybridization of the liquid component using a water-soluble monomer system, namely, hydroxyethyl methacrylate (HEMA); the resulting cements are referred to as hybrid ionomeric cements (HICs). HEMA undergoes ambient free-radical polymerization, and cement maturation is achieved via a dual-cure set, resulting in the retention of the components within a single phase [2]. This dual-cure nature and the reduced moisture sensitivity have enhanced the applicability of these cements for the treatment of gingival and subgingival lesions.

A key advantage of GCs is their bioactive nature. Characteristically, the remineralization effect is mediated via ion release from the glass core in the set cement matrix. Because the bioactivity of cement is based on ion exchange from the "glass core–gel matrix" structure, the acid–base reaction within the cement becomes vital. While conventional GCs exhibit efficient ion exchange after the near completion of the chemical reaction, HICs are limited by their complex dual-cure nature. Because of the dual-cure mechanism, a network competition behavior is exhibited between the acid neutralization and free-radical reactions [3, 4]. Furthermore, the proportional substitution of water with the monomer for the hybridization of the reaction liquid retards acid neutralization [5]. Therefore, the polyacid reaction within the HIC matrix is predisposed to underexpression and, subsequently, reduced epitaxial and cellular bioactivity.

Polybetaines are a group of zwitterionic derivatives with biofouling resistance and are, thus, used extensively in various biomedical applications [6]. Zwitterions are small molecules with a covalent linkage between the cations and anions, resulting in a structure with a large dipole. This dipole can be readily tuned using a combination of derivatives and has recently been shown to have a network-modifying action on GCs [7]. In contrast, the

[a] Department of Orthodontics, Institute of Craniofacial Deformity, Yonsei University College of Dentistry, 50-1 Yonsei-ro, Seodaemun-gu, Seoul 03722, Republic of Korea.
[b] Department and Research Institute of Dental Biomaterials and Bioengineering, Yonsei University College of Dentistry, 50-1 Yonsei-ro, Seodaemun-gu, Seoul 03722, Republic of Korea.
[c] Department of Oral Microbiology and Immunology, School of Dentistry and Dental Research Institute, Seoul National University, Seoul, 08826, South Korea
[d] BK21 FOUR Project, Yonsei University College of Dentistry, 50-1 Yonsei-ro, Seodaemun-gu, Seoul 03722, Republic of Korea
‡ These authors contributed equally to the article.
*Corresponding authors.
Electronic Supplementary Information (ESI) available: [details of any supplementary information available should be included here]. See DOI: 10.1039/x0xx00000x

setting reaction chemistry of HICs is complex and challenged by alteration of energetics owing to the inclusion of HEMA [8]. Recent studies have reported that zwitterions have a nonlinear boosting effect on the dielectric constant, which is attributable to the dipole [9]. As the main deterrent to the acid–base reaction of HICs is the low dielectric constant, which reduces the activity of acrylic acid, we hypothesized that the addition of polybetaine in different combinations would aid the setting reaction because of the resulting compensation. Furthermore, the network-modifying action of zwitterionic derivatives would enhance ion release and improve both epitaxial and biomimetic remineralization [10].

The general therapeutic application of HICs is such that it experiences two interfaces: dynamic multispecies interaction at the external surface, and an interior dentinal reparative end.

Resisting microbial insult will aid in longevity of the cement, while stimulation of underlying cell rich region can help in regeneration. Adult postnatal human dental pulp stem cells (hDPSCs) are precursors for the cellular repair of dentine and lead to the formation of dentine-like mineralized tissues [11, 12]. As HICs are applied at various depths from the vascularized pulpal region. Ionic diffusion through hypomineralized dentine can provide the necessary stimulation to hDPSCs, as demonstrated by Huang et al. [13].

Given the facts stated above, in this study, we used a strontium-fluoroaluminosilicate powder based HIC to analyze the modifying influence of polybetaines. The objectives of the study were to (1) incorporate polybetaine combinations within the liquid phase in varying ratios, (2) analyze the effects of the polybetaine combinations on the competitive setting reaction of the dual-curing process, (3) compare the ion-release behaviors and effect on stimulation of hDPSCs and (4) to investigate the zwitterion-mediated multispecies biofilm resistance. Finally, we evaluated the dysbiosis resistance response with 16s amplicon sequencing.

Experimental

Preparation of polybetaine-modified HICs

The polybetaines used, namely, 2-methacryloyloxyethyl phosphorylcholine (MPC) and sulfobetaine methacrylate (SB), were purchased from Sigma-Aldrich. The HIC experimental groups were defined (Table S1) based on the MPC/SB (*m*ZM) [7] ratio used, as follows: CTRL (no *m*ZM) , alpha (α–*m*ZM, MPC:SB = 1:1), beta (β–*m*ZM, MPC:SB = 1:2), and gamma (γ–*m*ZM, MPC:SB = 2:1). The glass (Fuji II LC, GC Corp., Tokyo, Japan, Shade A2, Lot 2008051) formed the powdered phase, while the liquid consisted of HEMA (30%–40%) and polyacrylic acid (20%–30%) in an aqueous solution (Fuji II LC, GC Corp., Tokyo, Japan, Shade A2, Lot 2008051)[14]. The *m*ZMs were homogenized into the liquid component in a 3% mass fraction at 3500 rpm (Speed mixer; DAC150.1 FVZ, Germany). All the samples used for testing were fabricated by mechanical mixing (3500 rpm) and light-cured for 40 s (Figure S1).

Characterization of polybetaine-modified HICs

Fourier-transform infrared spectroscopy (FTIR) was used to examine the structures of the HICs during setting. The procedure employed was adapted from a previously published method [14]. All the spectra were recorded by performing 32 scans at a resolution of 4 cm^{-1}. Baseline correction was performed, and the normalized absorption intensities of the peaks in the 800–3500 cm^{-1} range were compared. Immediately after components had been mixed, the contiguous pastes were placed over the diamond element within a 10 mm × 1 mm area and covered with an opaque lid. Next, the spectra were recorded; these spectra are referred to as the preirradiation spectra. For standardization, all the preirradiation spectra were recorded 120 s after mixing. Subsequently, the samples were light-cured for 40 s [14], and their spectra were recorded at 2-min intervals, with the last set of spectra recorded 10 min after the start of the mixing process. The recorded spectra represent the average of three measurements for each group. The tested samples were subsequently immersed in simulated body fluid (SBF, pH = 7.45), and their spectra were recorded again after immersion for 7 and 14 days. The acid–base reaction efficiency was determined from the averaged spectra using a previously described method [15, 16]. Briefly, the complex ester peaks at 1712 cm^{-1} were deconvoluted into three subpeaks viz. 1740 cm^{-1} (representing the unionized carboxyl groups), 1704 $cm^{-1}$and 1712 cm^{-1} (representing substitution dependent ester groups). The ratio of the height of peak related to the metal-carboxylate salt (COOM, at approximately 1500–1600 cm^{-1}) to that of the peak related to the unionized remnant carboxyl groups) was calculated. Next, all the spectra were baselined, smoothened, and analyzed using SpectraGryph (version 1.2) [17].

The surface morphologies and subsurface elemental compositions of the samples were studied by field-emission scanning electron microscopy (FESEM) using a JEOL-7800F microscope (Tokyo, Japan) equipped with an energy-dispersive X-ray spectrometry (EDS) attachment.

Ion-release profiles in SBF

The ions released from the HIC groups were monitored at 37 °C for 14 days. The HIC samples were prepared using disc-shaped metal molds (10 mm in diameter × 2 mm in thickness). The average weight of the polished (P2000 macro grits) samples was 0.36 ± 0.02 g. The polymerized discs were soaked in SBF (5 mL, pH = 7.4) at 37 °C. The number of ions released was measured using inductively coupled plasma atomic emission spectrometry (Agilent 5100, Agilent Technologies, CA, USA) after 7 and 14 days of immersion. The fluoride ion concentration was assessed using a 920A electrode (Orion, Boston, USA). Three samples were used for each experiment, with a minimum of three reads per sample.

Cell culture

Cryopreserved hDPSCs (Poietics™, Lonza, Walkersville, MD, USA) were used in the present study. According to the supplier (Lonza walkjersville, INC, USA) the cells were sourced from a single, 21-year-old male, donor and expressed of cluster differentiation factors (CD $CD105^+$, $CD166^+$, $CD29^+$, $CD90^+$,

CD73^{+}, CD133^{-}, CD34^{-}, CD45^{-}) with flow cytometry. The cells cultured from third passages were used for analyses in the present study.

Evaluation of cytocompatibility (MTT assay)

The cytotoxicity of the samples was determined using a 3-(4,5-dimethylthiazol-2-yl)-2,5-diphenyltetrazolium-bromide (MTT; Sigma-Aldrich, St. Louis, MO, USA) assay in accordance with the ISO 10993-5 and -12 standards. The hDPSCs were kept at 37 °C in a humidified incubator under 5% CO_2 in Dulbecco's modified Eagle's medium (DMEM) supplemented with 10% fetal bovine serum (Gibco Life Technologies, USA). The cells were seeded (1×10^4 cells/well) in a 96-well plate and incubated for 24 h. The HIC test specimens were formed under aseptic conditions using a sterile cylindrical mold (10 mm × 2 mm) and sterilized by ultraviolet irradiation for 30 min. Extraction was performed at a rate of 3 cm^2/mL, and the extract was filtered through a 0.22-µm syringe filter. The filtered extract was then added to the cells in different concentrations (100%, 50%, 25%, and 12.5%). After 24 h, the cells were incubated at 37 °C in the dark in the MTT solution. After 2 h, the MTT solution was carefully removed, and 100 µL of dimethyl sulfoxide (0231, VWR Life Science, Radnor, PA, USA) was added to each well. The optical density was measured at 570 nm using a plate reader (Epoch, BioTek, Winooski, VT, USA). All the experiments were performed thrice.

Response of hDPSCs to bioactivity of α-*m*ZM

The primary response of the hDPSCs, described in the subsections that follow, was determined from cumulative HIC eluates (14-day) obtained using 0.1 cm^3/mL of DMEM (Gibco, Carlsbad, CA, USA); the analysis was performed at 37 °C in 5% CO_2 with 95% humidity [18]. All the tests were performed on a minimum of three samples.

The method used was adapted from the protocol described by Huang et al. [13]. The cultured cells were fixed with ice-cold 4% paraformaldehyde on day 14 and permeabilized with 0.2% Triton X-100 for 10 min. Nonspecific binding was blocked using 10% donkey serum. Primary antibodies: dentine sialophosphoprotein (DSPP, origin: Rabbit) (1:50 dilution) and dentine matrix protein 1 (DMP-1, origin: mouse) (1:100 dilution) was then added for 1 h at room temperature, and this was followed by incubation with a specific secondary antibody (Alexa Fluor 568 or Alexa Fluor 488) for 1 h at 37 °C. Next, the nuclei were counterstained with 4',6-diamidino-2-phenylindole (DAPI). The cells were then washed and viewed under a confocal microscope (LSM880, Carl Zeiss, Thornwood, NY, USA). The recorded images were analyzed, and the fluorescence intensity was quantified (geometric mean) using the software ZEN (version 3.4, Blue edition, Zeiss).

The alkaline phosphatase (ALP) activity of the hDPSCs was evaluated by spectrophotometric analysis performed using a substrate p-nitrophenylphosphate (pNPP, Sigma-Aldrich) assay kit at day 14, in accordance with a previous study [19]. The cells were lysed using a protein lysis buffer without a protease inhibitor, and the cellular ALP activity was assessed by incubating the protein lysates with pNPP at 37 °C for 30 min. The reaction was analyzed based on the colorimetric quantification of the absorbance at 405 nm, and normalization was performed based on the corresponding protein amounts.

The degree of mineralization of the extracellular matrix was evaluated using Alizarin Red staining (ARS), which was performed on the hDPSCs at day 28. To quantify the ARS assay, we adapted a previously described protocol [19]. Briefly, the adherent hDPSCs were fixed with ice-cold 70% ethanol for 1 h after three PBS washes. Next, an ARS solution (40 mM, pH 4.2, Sigma-Aldrich, St. Louis, MO, USA) was used to stain the cells. The staining solution was removed by washing the cells multiple times with PBS. Images showing the mineralization of the extracellular matrix of the stained cells were captured using a light microscope. To quantify the degree of mineralization, the AR-stained cells were eluted with 10% cetylpyridinium chloride (Sigma-Aldrich), and quantification was performed through spectrophotometric analysis based on the absorbance at 562 nm.

Quantitative real-time polymerase chain reaction (qPCR)

The gene expression levels were measured under dynamic refreshing conditions to emulate the conditions for clinically relevant biointeractions [18]. The eluates were sampled as described above; the difference was the introduction of an additional step involving refreshing the medium after 72 h. The eluates were collected after 24 h, 7 days, and 14 days and analyzed for gene expression at a concentration of 50% based on the cell viability results. The total RNA was extracted using the RNeasy Mini Kit (Qiagen, 74140). The cDNA was synthesized using SuperScript III First Strand with oligo-dT primers (Invitrogen, 18080-051) as per the manufacturer's instructions. The SYBR Green PCR master mix (Applied Biosystems, 4309155) and CFX Connect™ Optics Module (Bio-Rad Laboratories, 788BR06586) were used for the qPCR analysis. The cycling parameters for the PCR were as follows: 95 °C for 15 min, 95 °C for 10 s, 60 °C for 15 s, and 72 °C for the 30 s for 40 cycles, followed by 72 °C for 10 min and 95 °C for 10 s. The relative gene expression levels were quantified using the delta Ct method. The primers used in this study are listed in Table 1.

Table 1. Primers used for qPCR

Gene	Sequences (5'–3')
RUNX2 (Runt-related transcription factor 2)	F: AAC CCT TAA TTT GCA CTG GGT CA R: CAA ATT CCA GCA ATG TTT GTG CTA C
OCN (Osteocalcin)	F: CCC AGG CGC TAC CTG TAT CAA R: GGT CAG CCA ACT CGT CAC AGT C
OPN (Osteopontin)	F: ACA CAT ATG ATG GCC GAG GTG A R: TGT GAG GTG ATG TCC TCG TCT GTA G

***Ex vivo* analysis of resistance to multispecies biofouling**

After obtaining approval from the Ethics Committee (IRB No. 2-2019-0049), we collected saliva samples from six individuals.

The samples were mixed, and biofilm analysis was performed using a protocol described elsewhere [7]. Briefly, McBain broth medium (1.5 mL) and the collected saliva samples were mixed (50:1) and dispensed into wells containing the test specimens (10 × 2 mm). The samples were stored at 37 ℃ in a 5% CO_2 incubator, and the medium was changed after 8 and 16 h. The samples were incubated for 24 h after the last medium change [20]. Next, the specimens were gently rinsed in distilled water and stained using a live/dead bacterial viability kit (Molecular Probes, Eugene, OR, USA). Confocal laser scanning microscopy (CLSM; LSM980, Carl Zeiss, Thornwood, NY, USA) was performed to image the stained biofilms. The biofilm thickness was calculated using the software Zen (Carl Zeiss, Thornwood, NY, USA), and the average biomass was determined using the COMSTAT plug-in (Technical University of Denmark, Kongens Lyngby, Denmark) of ImageJ [21].

16s rRNA sequencing

Genomic sequencing was performed to identify the compositions of the biofilms formed on the CTRL and α-*m*ZM HIC samples. The saliva (sample collection same as exvivo multispecies experiment) was mixed and cultured on the specimens using the method described in the previous section and analyzed according to a previously published protocol [22]. Briefly, the extracted DNA samples were amplified via the polymerase chain reaction (PCR) with primers targeting the V3–V4 regions of the 16S rRNA gene. Amplicon sequencing was performed using an Illumina MiSeq Sequencing System (Illumina, USA). The low-quality reads (<25) were filtered and merged paired-end sequence data were generated. Unique reads with a similarity threshold of 97% were isolated for taxonomic allocation based on the EzBioCloud 16S rRNA database [23]. Downstream analyses were performed using web-based tools [23-25].

Statistical analysis

Each experiment was performed at least thrice. The results are expressed as the mean, and the standard error was analyzed statistically by one-way analysis of variance (ANOVA). Post-hoc analysis for comparison between groups were performed using Tukey's test for biomass comparison and Scheffé's post-hoc test for ion release profile (SPSS 20.0). The scores corresponding to the biological responses of the hDPSCs were subjected to the t-test. The differentially abundant species were compared by performing a linear discriminant analysis (LDA) to evaluate the size effect using a threshold LDA score of ≥2 [26]. Values with $p < 0.05$ were considered statistically significant.

Results and discussion

Changes in HIC setting behavior with addition of polybetaine

The wide acceptability of HICs comes at the expense of an inherent network competition within the cement matrix. The setting reaction progresses through two simultaneous but distinct pathways, namely, acid neutralization and monomer-to-polymer conversion. The effects of these two reaction pathways are complex and often have a determining effect on the final properties of the cement. In order to elucidate the network-modifying effect of polybetaines, we explored the changes in the HIC setting reactions using attenuated total reflection FTIR (**Figure 1**). The baseline-corrected spectra were evaluated both before and after photoirradiation in the dry state. The spectra obtained before irradiation showed relatively higher absorbance peaks corresponding to the stretching of the S=O bonds (~1350–1400 cm^{-1}) [27] and the phosphoryl halide groups (~1295 cm^{-1}) [28] of the *m*ZM groups (Figure S1). These spectra confirmed the successful incorporation of the polybetaine groups, namely, MPC and SB, which were included in different proportions, as can be seen from **Figure 1**A (see inset). The difference in polybetaine proportion is also observed in the phosphoryl halide groups with γ-*m*ZM showing highest absorbance. After irradiation, the peak related to the stretching of the C=C bonds of methacrylate (~1633 cm^{-1}) exhibited a characteristic decrease in intensity. The *m*ZM groups showed near-identical absorbances, which were only slightly different from those of CTRL, suggesting the degrees of polymerization of the different groups were similar. The fabricated samples were also similar in appearance, which was not affected by the polybetaines. In other words, the characteristic features of the HIC were maintained (Figure S2). We also confirmed the differential acid–base reaction ratio using IR spectroscopy after irradiation, matching 600 s after the mixing standard. As the reaction that occurs within the matrix of HICs is competitive, the elapsed time between the mixing and curing processes affected the IR results [14]. Therefore, we evaluated the changes in the COOM/COOH ratio after 600 s (**Figure 1**B). All the groups exhibited a similar ratio, which was approximately 1. These observations are in keeping with those of Kakaboura et al. [15], who reported a low differential ratio after irradiation. However, in this study, we attempted to simulate clinically relevant scenarios and thus performed additional examinations after 7 and 14 days of immersion in SBF. In contrast to the case for the initial observations performed immediately after immersion in SBF, after the delay, the *m*ZM groups exhibited an increased COOM/COOH ratio. For instance, after 7 days, the ratio ranked as α-*m*ZM ≈ β-*m*ZM > γ-*m*ZM > CTRL, while after 14 days, they could be arranged as α-*m*ZM > β-*m*ZM ≈ γ-*m*ZM > CTRL. Thus, α-*m*ZM showed the highest number of cross-links after 14 days of immersion in SBF, while the change in the case of CTRL was the smallest. Because the reaction features were explored cross-sectionally, a more definitive conclusion regarding the reaction rate cannot be made at this point. However, a reduction in the rate of COOM formation with an increase in the COOM/COOH ratio has been reported previously as well [16, 29]. The HIC formulations show 17 times difference in initial reaction rate in comparison to conventional first-generation cements, with the difference being primarily attributable to the reduced water content of the formulations [29]. However, HICs can exhibit slow continuation of internal reaction, which is initiated by water sorption. Because zwitterionic derivatives are better at holding water, it is plausible that the increase in the ratio after immersion in SBF is attributable to the surrounding water. Thus,

it can be expected that the reaction would continue to occur even under actual conditions. Lastly, we conducted a surface analysis of the various samples after aging for 3 days under constant relative humidity conditions (**Figure 1**C-D and Figure S3). Elemental mapping performed simultaneously revealed that the samples exhibited similar profiles, with their surfaces dominated by the glass-phase elements Sr and Al. In addition, low-intensity peaks related to F and P were also observed along with peaks related to oxygen (Table S2). Finally, the images indicated that all the samples had similar undulating surfaces.

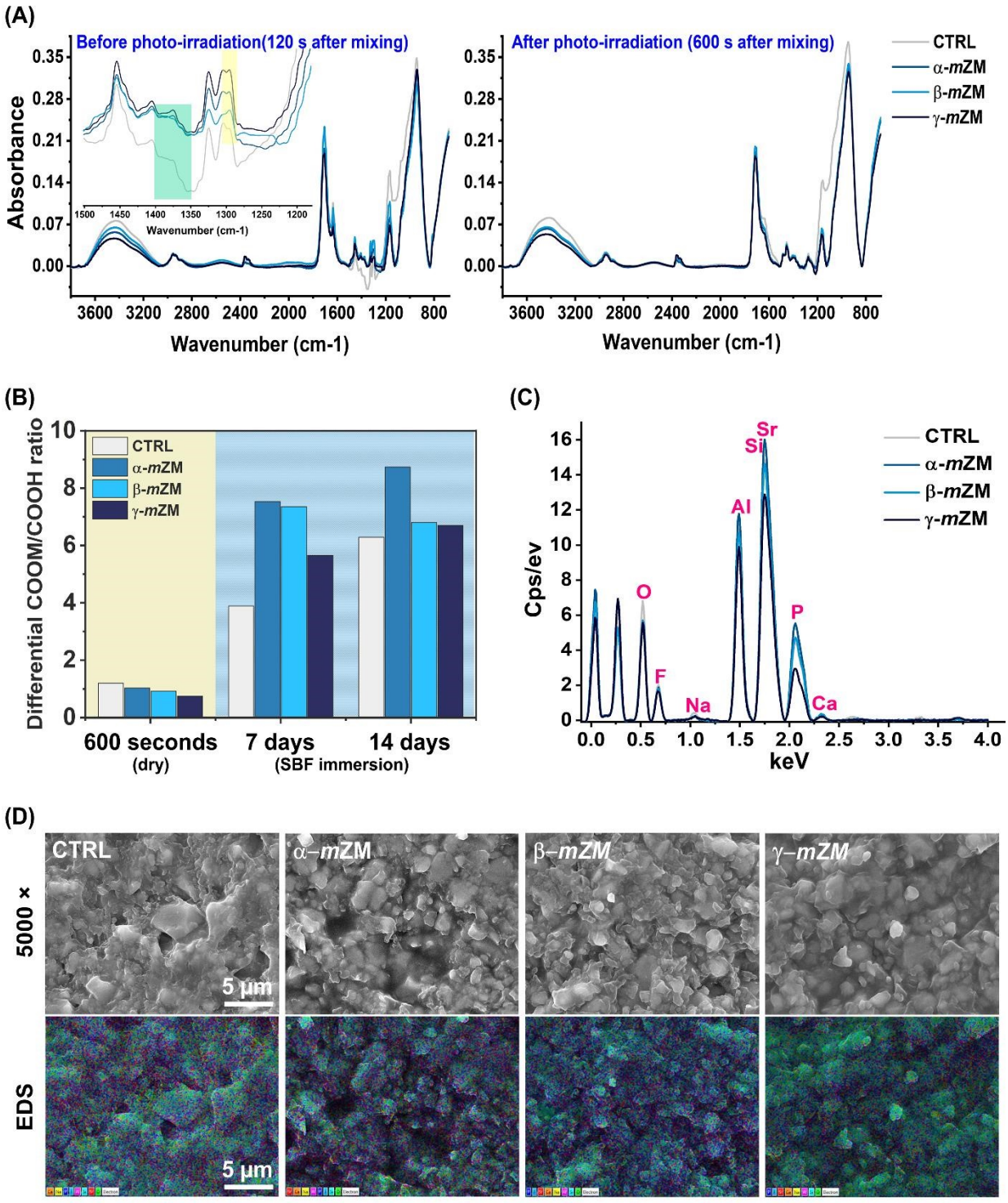

Figure 1. Characterization of hybrid ionomer cements (HICs). **(A)** Fourier-transform infrared spectroscopy (FTIR) spectra of HICs before (120 s after start of mixing) and after photoirradiation (600 s after start of mixing). Inset in first image shows spectra for wavenumber range of 1200–1500 cm^{-1} and highlights phosphoryl halide (yellow) and S=O (green) absorbance regions. Full scale figure is supplemented as Figure S1B. **(B)** Differential COOM/COOH ratios of specimens in dry state (after 600 s) and after immersion in simulated body fluid (SBF) for 7 and 14 days. **(C)** and **(D)** Energy-dispersive X-ray spectroscopy (EDS) mapping spectra of surfaces of HIC specimens and corresponding electron microscopy images. Scale bar is 5 μm.

View Article Online
DOI: 10.1039/D2BM01428A

ARTICLE

Polybetaine modification improves cumulative release of constituent ions

The core glass structure of HICs endows them with a fundamental ion-releasing nature. The exchange of fluoride ions is the primary mechanism responsible for the remineralization of carious lesions [30]. The ion-release behavior of ionomer cements during immersion in different media over varying periods has been studied extensively [31]. Their acid neutralization response is also well documented and is responsible for their high biocompatibility [7]. Previous studies have also explored the role of polybetaines in aiding the neutralization of bioactive resin formulations and have attributed it to enhanced ionic exchange from the bioactive filler[32, 33]. In accordance, we investigated the cumulative ion-release and contrasted CTRL against the *m*ZM groups. Because it has reported previously there is an increase in elution at lower pH values (distilled water, *ca.* 5.45)[7], we aimed to determine the cumulative amounts of ions released for a neutral starting pH (SBF, *ca.* 7.45). The optical properties of the HIC formulation investigated in this study are tuned to ensure good aesthetics. Hence to achieve aesthetic superiority the calcium component, which is more opaque, was replaced with Sr, making the latter the primary component of HIC glass network (*ca.* Sr/Si = 2.67, Ca/Si=0.01) [15]. In the present study the observed results were in accordance and reflected the primary components after 7 and 14 days (Figure **2**A-B). An enhancement of the release of Sr, F, and Si ions was observed for all the *m*ZM groups, with the released amounts being significantly higher ($p < 0.05$) than those for CTRL. As the concentration of Ca and P in HICs is inherently low, there was no significant difference in the released amounts of ions of these elements. The small differences seen between the groups might be resultant of intrinsic SBF composition (Figure 2C-D). Although a static cumulative concentration differs from the clinical application, the analysis allowed for a comparison at a pH similar to physiological range. Nevertheless, additional studies accounting for pH fluctuations will add to understanding the ion exchange mechanisms.

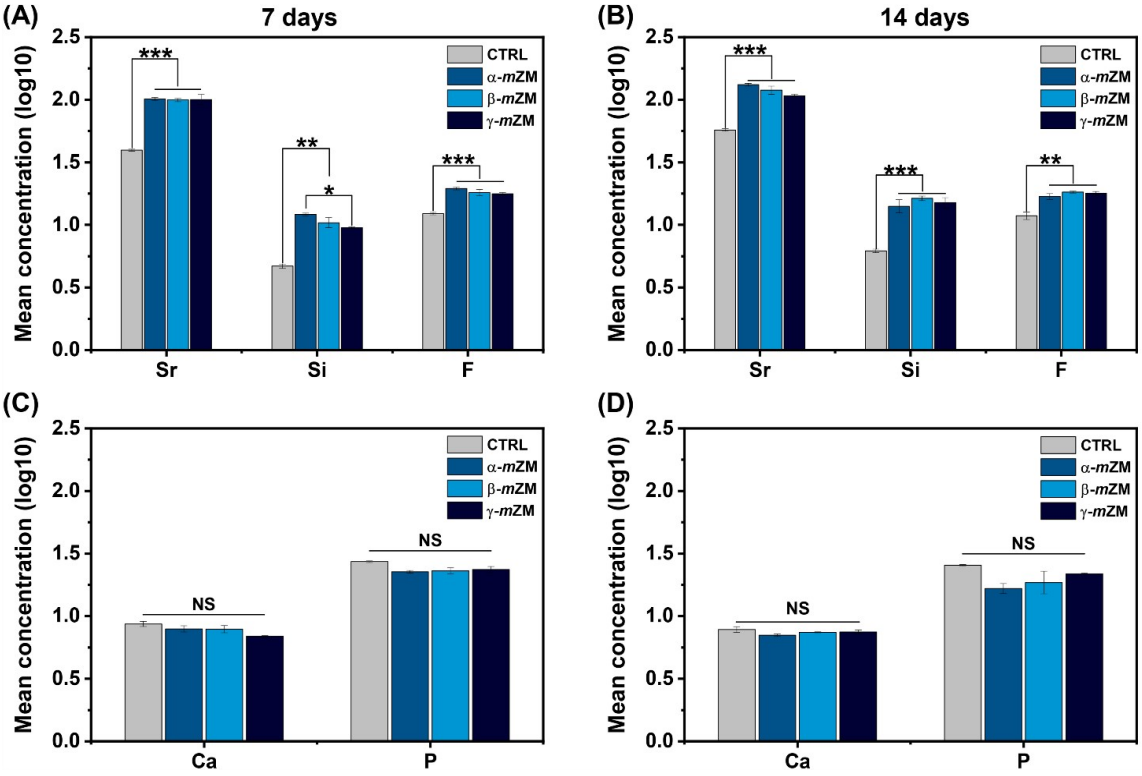

Figure 2. Cumulative ion-release profiles of HIC samples after 7 and 14 days. Statistically significant increases in cumulative concentrations of Sr, Si, and F ions with respect to those for CTRL were observed after both (A) 7 and (B) 14 days. Cumulative concentrations of Ca and P ions after (C) 7 and (D) 14. Y-axis uses log10 scale for cumulative ion concentrations (in mg/L). One-way ANOVA and post-hoc Scheffé's test were performed (n = 5, *p < 0.05, **p < 0.01, ***p < 0.001, NS; not significant).

View Article Online
DOI: 10.1039/D2BM01428A

Response of hDPSCs to *m*ZM modification

The bioactivity of glass-based cements is primarily attributable to the release of ions from the core matrix. The polybetaine-*m*odified HIC samples displayed markedly increased Sr, Si, and F ion secretion during incubation in SBF. hDPSCs represent a heterogeneous multipotent cell population enclosed within loose connective tissue, and their angiogenic healing nature is supported by observations of the perivascular region of the pulp ("pericytes") [34]. Moreover, the therapeutic application of HICs occurs in the immediate vicinity of the hypomineralized dentine region, allowing for the deep penetration of the ions released from the cement interface. Hence, a subsequent stimulatory effect occurs in the subjacent cellular region. Therefore, in this study, we evaluated the response of hDPSCs to the collected ionic elutes. The cellular responses were compared to that of a static eluate (Figure 3). In addition, to ensure therapeutic relevance, a dynamic eluate was also tested, as shown in Figure 4.

Using an initial cell viability assay, we evaluated the cytocompatibility at various concentrations (Figure 3A). We aimed to present an objective comparison between the modifications against CTRL by emphasizing the concentration-dependent response. The test concentration for all subsequent assays was based on the highest viability response for CTRL (50%). Similar results were reported in a recent clinical study, showing compatibility of HICs in deep tooth cavity linings.[35] With no significant difference in cytocompatibility results against CTRL, and being well above 70% ISO threshold, we could validate that *m*ZM modification did not adversely affect the material behavior.

Furthermore, based on the above results, we compared the α-*m*ZM group with CTRL for expression of markers of cellular bioactivity. The results of immunohistochemical staining with DMP-1, DSPP and DAPI are shown in Figure 3B-C. During dentine formation, DSPP is proteolytically cleaved into smaller subunits, such as dentine sialoprotein and dentine phosphoprotein (DPP), and DPP plays an important role in biomineralization, and DMP-1 forms the putative marker in odontoblastic bioactivity [36] An increased expression of DSPP is indicative reparative dentine formation response being the specific odontoblastic differentiation marker.[37] In the present study, we observed a 32.5% increase in intensity of DSPP via immunocytochemistry with α-*m*ZM HIC, indicative of stimulatory response from increase ion elution. Similarly, a marked increase (*ca.* 245%) in DMP-1 was also observed in the α-*m*ZM group. Increase in DMP-1, component of mineralizing extracellular matrix of bone, was also a promising indicator for cellular stimulation directed towards dentine formation (Figure 3D). A recent study also reported a similar increase in DSPP expression, highlighting the role played by increase Sr ion concentration. The researchers concluded that the increased DSPP expression was indicative of hDPSC mineralization [13]. Given that Sr, which is the principal component of the tested HIC samples, was observed in increased concentrations in the α-*m*ZM elute, it is possible that a similar mechanism led to the increased expression of odontoblast related markers. α-*m*ZM also exhibited significantly enhanced ($p < 0.001$) biomineralization during the ARS analysis after 28 days of culturing (Figure 3E). However, at 14 days, the ALP activity relative to the total protein expression showed only a minor increase, which was statistically not significant ($p = 0.26$) (**Figure** S4A)

View Article Online
DOI: 10.1039/D2BM01428A

ARTICLE

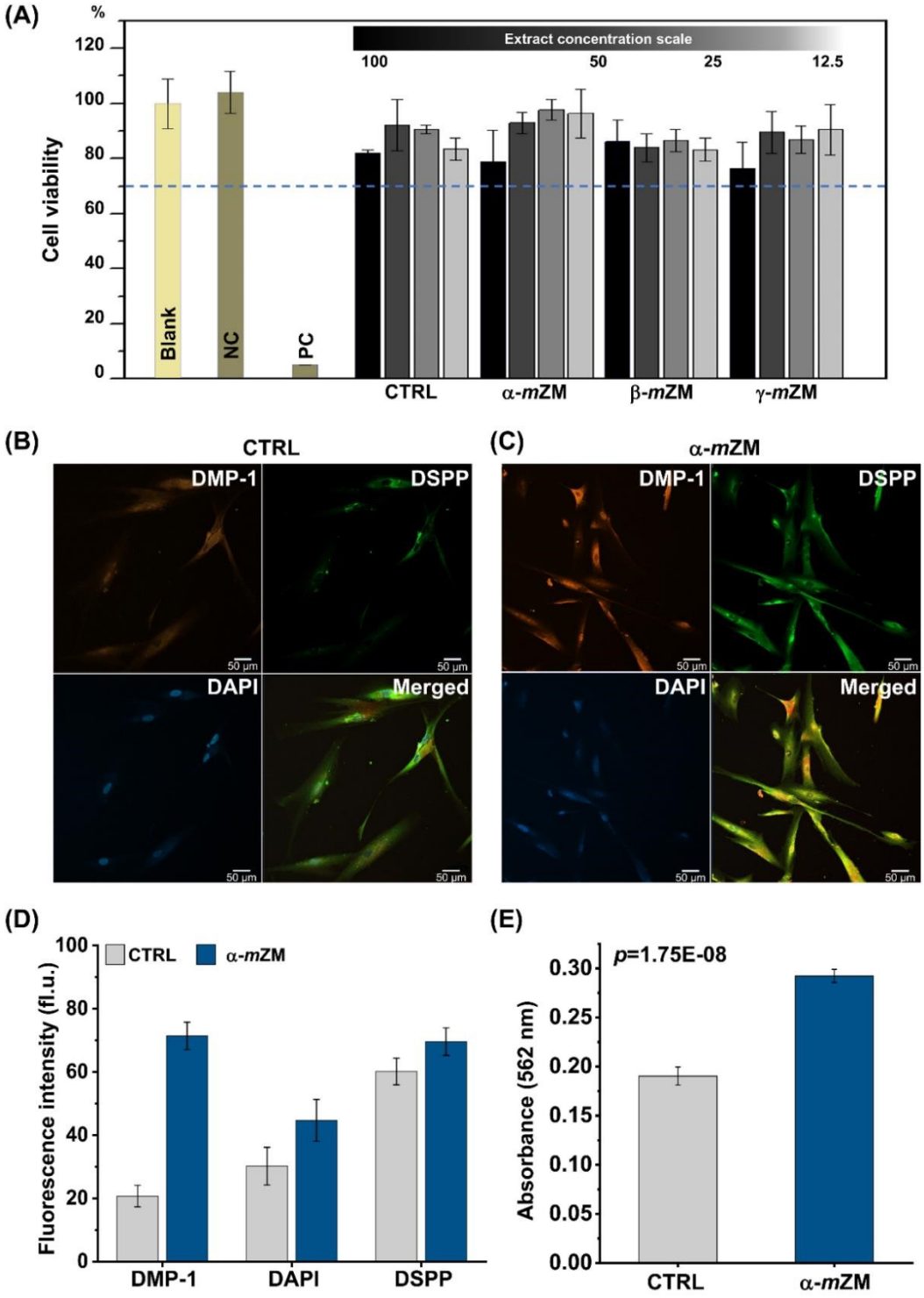

Figure 3. Response of human dental pulp stem cells (hDPSCs) to cumulative 14-day eluates. (A) Cell viability analysis of experimental groups for different concentrations as per ISO10993-12; blue dotted line represents acceptable 70% threshold. (B-C) Representative immunocytochemistry images stained hDPSCs for (B) CTRL and (C) α-*m*ZM groups (n = 5); scale bar is 50 µm. (D) Corresponding fluorescence intensity measures (geometric mean). (E) Alizarin-red-normalized absorption of hDPSCs after 4-week culture. *p* value is indicated in panel for statistical comparison with Student's t-test. PC; positive control (0.5% phenol solution), NC; negative control (high-density polyethylene), CTRL; cement group without polybetaine modification.

The cell proliferation assay (Figure S4B) showed that α-*m*ZM exhibited a significant increase in hDPSCs ($p < 0.05$) after 4 days; however, after 7 days, the levels of α-*m*ZM and CTRL were comparable. This variation could be attributed to an initial early response in cell maturation. To further characterize the behavior, we examined the gene expression of hDPSCs in a growth medium for extracts obtained at different intervals as schematically presented in Figure 4A. The mRNA expression levels of RUNX2, OCN, and OPN were selected as the phenotypic markers. RUNX2 is a transcription factor and regulator of gene expression during odontoblast differentiation [13], while OCN and OPN are synthesized by maturing odontoblasts and osteoblasts, which are regarded as late cell differentiation markers [38, 39].The relative expression analysis performed using qPCR showed significantly increased ($p < 0.01$) levels of RUNX2, OCN, and OPN in the day-1 extracts of α-*m*ZM (Figure 4B). The expression of RUNX2 is indicative of the commitment of stem cell towards an odontoblast or osteoblast lineage. Additionally, RUNX2 promotes the binding of transcription factors to osteocalcin specific protein. [40] The highly significant increase in relative expression of RUNX2 and OCN from Day1 extracts also indicates hDPSC commitment to odontoblastic lineage. This trend was in sharp contrast to that for CTRL, which only exhibited increased expression levels after the last refresh cycle. Although, the expression in α-*m*ZM were higher than CTRL in Day7 extracts also, attributable to an improved ion release response. The bioactivity of cement is affected by the pattern of ion release from the GC in general follow a two-stage elution profile for inducers, exhibiting an initial rapid phase and a longer secondary phase. Moreover, the secondary phase is affected by the pH and is slower under neutral conditions [31]. Therefore, it is possible that the contrasting gene expression trends observed in this study are related to the augmented ion release with the addition of α-*m*ZM.

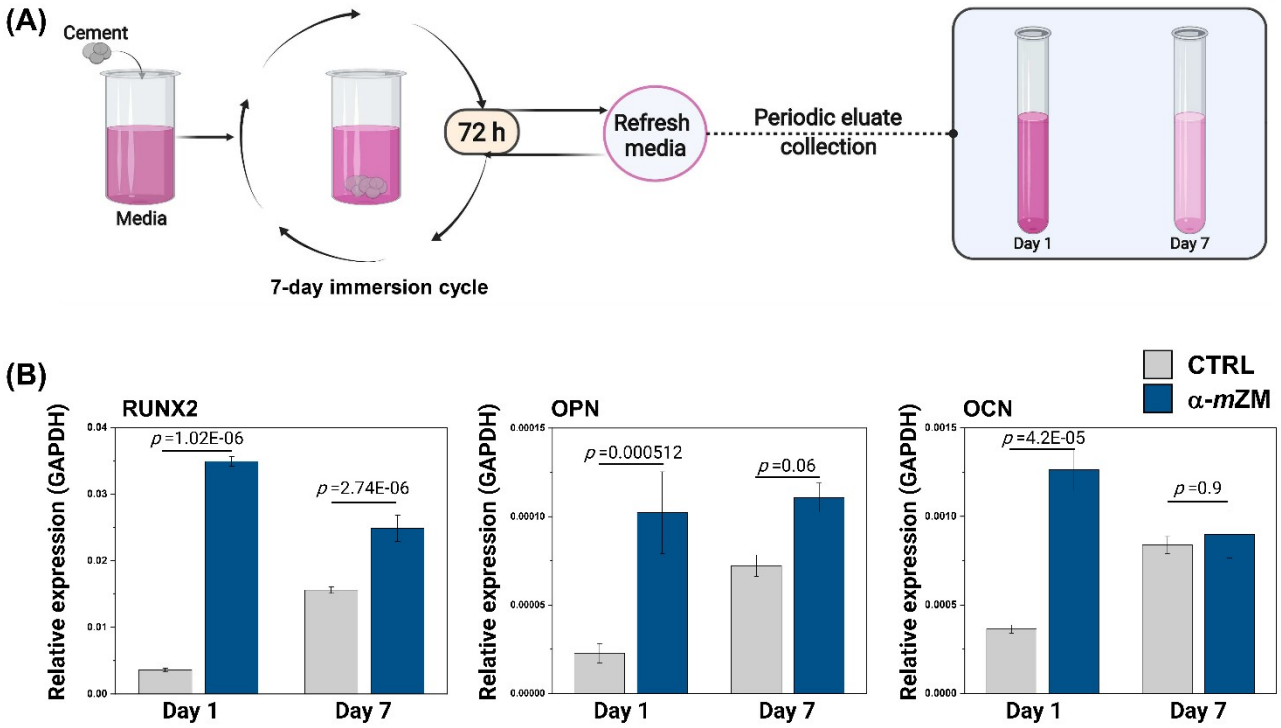

Figure 4. mRNA expression profiles of hDPSCs. Values shown are mean ± SE for three cultures. (A) Schema of experimental setup used to emulate clinically relevant scenario with regular refreshing of culture medium. Eluates were collected at three timepoints (on days 1, and 7) and evaluated for gene expression. (B) Relative gene expression levels for RUNX2, OCN, and OPN were measured in extracts corresponding to three timepoints. Dotted red line marks peak gene expression in CTRL on days 1 and 7. *p* values are indicated in panel for statistical comparison with Student's t-test.

View Article Online
DOI: 10.1039/D2BM01428A

Dysbiosis resistance and low biofouling with α-*m*ZM

The second desired biological effect is the improved resistance to microbiological insults which can lead to therapeutic failures. Oral plaque microcosms comprise more than 700 types of prokaryotes which forms the culture bed for multiple pathogenic species [6]. A notable functional effect of the investigated polybetaines, MPC, and SB, is their resistance to bacterial biofilms [32, 41]. In the present study, we tested the resistance of the various polybetaine combinations with respect to multispecies biofilm formation (Figure 5A). A clinically relevant setup was adapted for the ex vivo analysis of pooled human saliva. The *m*ZM groups showed significantly lower total biofilm thicknesses for a 72-h culture: α-*m*ZM ($p < 0.001$), γ-*m*ZM ($p < 0.01$), and β-*m*ZM ($p < 0.05$) (Figure 5B-C). Differential staining was performed, and the CLSM biomass ratios were calculated. The *m*ZM groups showed a marked reduction in the biomass in relation to that of CTRL, and their biomasses could be arranged as follows: α-*m*ZM > β-*m*ZM > γ-*m*ZM (ellipses, Figure 5B). Hence, it was concluded that α-*m*ZM exhibits the highest resistance to multispecies biofouling (Figure 5C). *m*ZM formulation comprising two polybetaines is believed to express a steric effect owing to the formation of an electrostatic hydration shell [6]. Furthermore, it is plausible that the non-zero structural effect, with the combination of MPC and SB, could improve the electrostatic interaction and subsequent biofouling resistance [7].

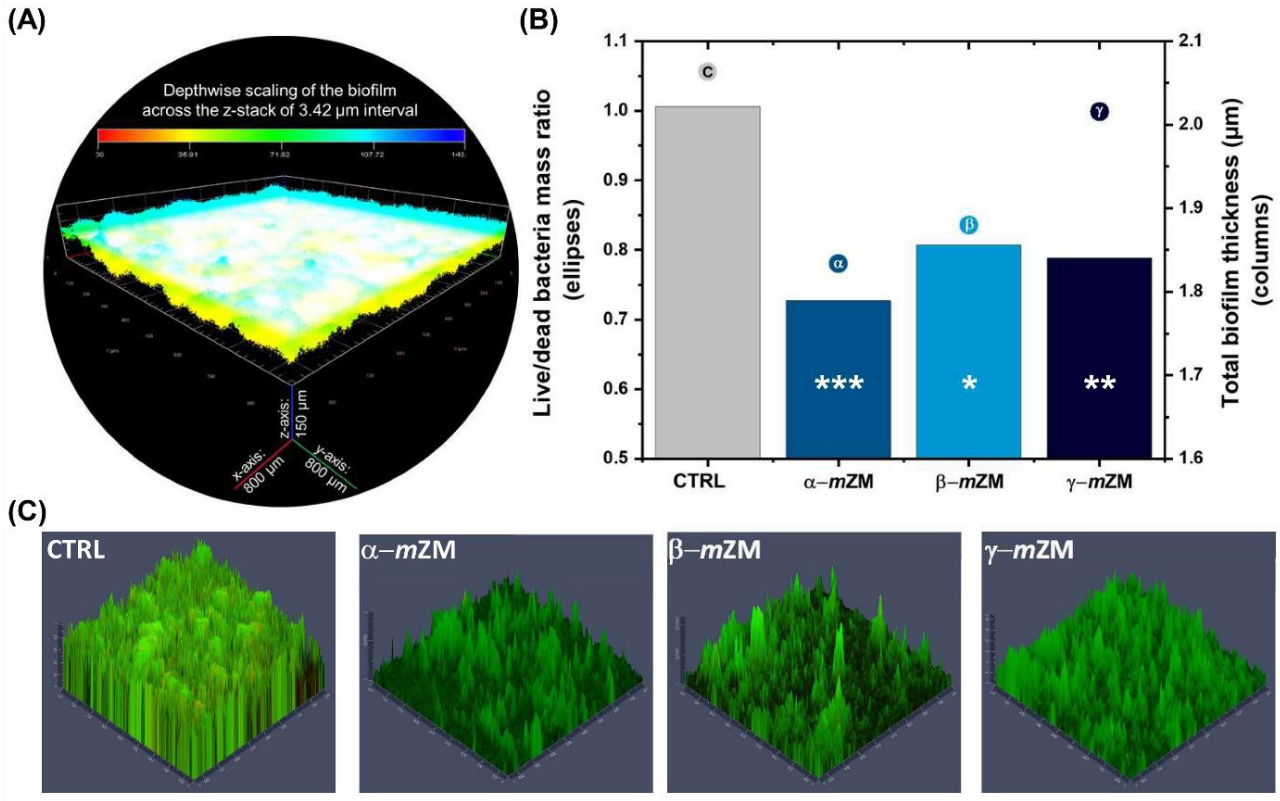

Figure 5. Resistance to multispecies surface biofouling. (A) Schema of biofilm evaluation by z-stack scanning using confocal laser scanning microscopy. Scans were performed at intervals of 3.42 µm for minimum of 150 µm (z-axis). (B) Biomass ratio of live (green fluorescence) and dead (red fluorescence) bacteria (ellipses) and biofilm thickness (columns). Y-axis uses log10 scale. Statistical analysis with ANOVA and post hoc analysis of Tukey's showed significant differences in biofilm thickness between *m*ZM groups and CTRL (n = 3, *$p < 0.05$, **$p < 0.01$, ***$p < 0.001$). (C) Confocal side-view images of biofilms formed over various samples.

View Article Online
DOI: 10.1039/D2BM01428A

Next, a detailed genomic characterization of the salivary biofilms cultured over the CTRL and α-*m*ZM samples was performed to determine the differences in their microbial diversity. It is known that 16s rRNA sequencing allows for an in-depth analysis of microbiota, including the unculturable ones. A comparison of the abundance profiles of the taxa allowed for the identification of the diversity patterns and differentially abundant taxa. The relative abundance ratios of the taxa in the CTRL and α-*m*ZM microbiomes were determined at three levels: phylum, genus, and species (Figure 6A). Although the richness and evenness indices for the two groups were similar (Figure 6B), significant differences (see Table S3, $p < 0.05$) were observed for five genera: *Veillonella, Streptococcus, Lactobacillus, Gemella,* and *Haemophilus* (Figure 6C). These results were similar to the microbiome profiles described for multispecies cultures of biomaterials [42, 43]. Further analysis revealed a significant reduction in *Veillonella sps.* in the case of α-*m*ZM, which was in sharp contrast to the mild-to-*m*oderate increase seen in the case of CTRL (Figure 6D). *Veillonella* consist of strictly anaerobic, gram-negative cocci, which act as bridging species in biofilm development both *in vivo* and *in vitro* and are highly abundant in saliva [44]. Hence, it can be concluded that the interference caused by α-*m*ZM, which significantly reduced the accessory and bridging species, such as *Veillonella*, probably have played a role in improving the biofouling resistance.

View Article Online
DOI: 10.1039/D2BM01428A

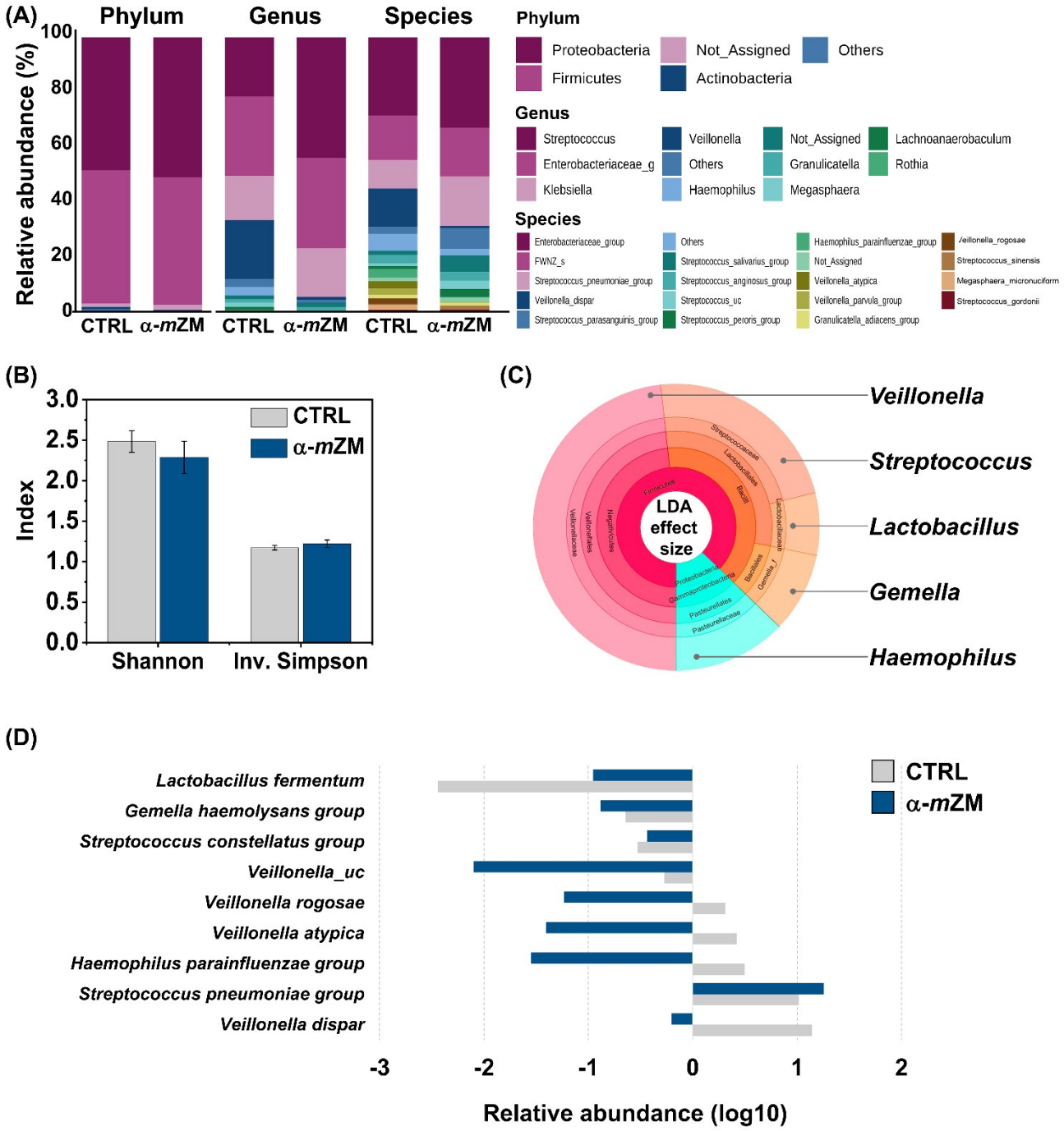

Figure 6. Microbiome abundance profiles of CTRL and α-*m*ZM samples. (A) Relative abundance percentages observed at levels of phylum, genus, and species. (B) Alpha diversity indices (Shannon's and inverse Simpson's) for comparing richness and evenness did not show any statistically significant difference (with Mann-Whitney U test). (C) Krona plot of significant taxonomic markers (LDA>2) identified based on linear discriminant analysis score and (D) comparison of relative abundances of various species.

View Article Online
DOI: 10.1039/D2BM01428A

The results obtained confirmed that it is possible to elicit a total biological response from HICs by including polybetaines in their setting chemistry, imparting initial ionic stimulation to underlying cells and resisting surface dysbiosis. Although, the results reflect the enhanced bioactive potential of the α-*m*ZM hybrid ionomers, the in vitro nature of the biomineralization experiments is self-limiting if one considers actual in vivo applications. Evaluations performed at multiple timepoints confirmed the augmented release of stimulating ions in improving cellular bioactivity; however, due multiple factors qRT-PCR does not offer high correlation to protein expression. Hence, based on the data available, it is not possible to determine the exact mechanisms involved. Moreover, in this study, we used a commercially approved HIC formulation. The commercial formulations are specific in the proportion of the constituent ions and the monomeric components. The predetermined ionic constituents can limit the bioactive response. Lastly, we observed a reduced mild variation in mechanical properties, highlighting the need to optimize constituent monomeric components with polybetaine to achieve stable properties. Nevertheless, we believe that the use of tailored compositions in future studies will allow for the release of different locally beneficial ions and hence elicit an even stronger bioactive response.

Conclusions

This study presented the effects of incorporating polybetaine zwitterionic derivatives into the HICs to investigate the bioactive effects epitaxially and through hDPSCs response. Based on results of the in vitro experiments performed in this study, it can be concluded that the polybetaine modification of HICs, that is, the use of the α-*m*ZM formulation, can promisingly contribute towards therapeutic improvements. The α-*m*ZM formulation is advantageous as it (i) enhances the release of the key constituent ions, namely, Sr, Si, and F, even at neutral pH; (ii) stimulates hDPSC cells; and (iii) improves resistance to biofouling and dysbiosis by limiting the colonization of the accessory species, thus enhancing their total biological effect.

Author Contributions

Utkarsh Mangal: data curation, writing–original draft preparation, visualization, formal analysis, investigation, writing–review, and editing. *Tae-Yun Kang:* data curation, methodology, investigation, formal analysis. *Ju Won Jung:* data curation, methodology, investigation, formal analysis. *Ji-Yeong Kim* and *Ji-Young Seo*: methodology, formal analysis, and investigation. *Jung-Yul Cha, Kee-Joon Lee, Hyung-Seog Yu* and *Kwang-Mahn Kim:* supervision, resources. *Jin-Man Kim:* resources, methodology, supervision, investigation, validation, writing–reviewing and editing, and funding acquisition. *Jae-Sung Kwon and Sung-Hwan Choi:* conceptualization, methodology, validation, supervision, project administration, writing–reviewing and editing, and funding acquisition. All authors have reviewed the manuscript. *U. Mangal* and *T-Y Kang* have co-first authorship based on equal contributions.

Conflicts of interest

The authors declare that they have no known competing financial interests or personal relationships that could have influenced the work reported in this study.

Acknowledgements

This work was supported by the National Research Foundation of Korea (NRF) grant funded by the Korea government (MSIT) (No. 2021R1A2C2091260 and 2022R1C1C1010304).

View Article Online
DOI: 10.1039/D2BM01428A

References

1. G. Mount, *Color atlas of glass ionomer cement*, 2002.
2. J. W. Nicholson, *Biomaterials*, 1998, **19**, 485-494.
3. A. Yelamanchili and B. W. Darvell, *Dent. Mater.*, 2008, **24**, 1065-1069.
4. D. W. Berzins, S. Abey, M. C. Costache, C. A. Wilkie and H. W. Roberts, *J. Dent. Res.*, 2010, **89**, 82-86.
5. A. M. Young, *Biomaterials*, 2002, **23**, 3289-3295.
6. U. Mangal, J. S. Kwon and S. H. Choi, *Int. J. Mol. Sci.*, 2020, **21**, 9087.
7. J. Y. Kim, W. Choi, U. Mangal, J. Y. Seo, T. Y. Kang, J. Lee, T. Kim, J. Y. Cha, K. J. Lee, K. M. Kim, J. M. Kim, D. Kim, J. S. Kwon, J. Hong and S. H. Choi, *Bioact. Mater.*, 2022, **14**, 219-233.
8. J. Nicholson and H. Anstice, *Journal of Materials Science: Materials in Medicine*, 1994, **5**, 119-122.
9. W. Mei, A. J. Rothenberger, J. E. Bostwick, J. M. Rinehart, R. J. Hickey and R. H. Colby, *Phys. Rev. Lett.*, 2021, **127**.
10. L. N. Niu, W. Zhang, D. H. Pashley, L. Breschi, J. Mao, J. H. Chen and F. R. Tay, *Dent. Mater.*, 2014, **30**, 77-96.
11. S. Gronthos, M. Mankani, J. Brahim, P. G. Robey and S. Shi, *Proc. Natl. Acad. Sci. U.S.A.*, 2000, **97**, 13625-13630.
12. S. Gronthos, J. Brahim, W. Li, L. W. Fisher, N. Cherman, A. Boyde, P. DenBesten, P. G. Robey and S. Shi, *J. Dent. Res.*, 2002, **81**, 531-535.
13. M. Huang, R. G. Hill and S. C. F. Rawlinson, *Acta Biomater.*, 2016, **38**, 201-211.
14. E. Dursun, J. F. Nguyen, M. L. Tang, J. P. Attal and M. Sadoun, *Dent. Mater.*, 2016, **32**, 640-645.
15. A. Kakaboura, G. Eliades and G. Palaghias, *Dent. Mater.*, 1996, **12**, 173-178.
16. B. Dickey, R. Price and D. Boyd, *Dent. Mater.*, 2016, **32**, 596-605.
17. F. Menges, 2020, **Version 1.2.15**, http://www.effemm2.de/spectragryph/.
18. X. Li, M. S. Pedano, S. Li, Z. Sun, C. Jeanneau, I. About, E. Hauben, Z. Chen, K. Van Landuyt and B. Van Meerbeek, *Mater. Sci. Eng. C Mater. Biol. Appl.*, 2020, **116**, 111167.
19. J.-H. Ryu, T.-Y. Kang, H. Shin, K.-M. Kim, M.-H. Hong and J.-S. Kwon, *Int. J. Mol. Sci.*, 2020, **21**, 8501.
20. W. Choi, S. Park, J. S. Kwon, E. Y. Jang, J. Y. Kim, J. Heo, Y. Hwang, B. S. Kim, J. H. Moon, S. Jung, S. H. Choi, H. Lee, H. W. Ahn and J. Hong, *ACS Nano*, 2021, **15**, 6811-6828.
21. C. A. Schneider, W. S. Rasband and K. W. Eliceiri, *Nature Methods*, 2012, **9**, 671-675.
22. D. S. Kim, Y. Park, J. W. Choi, S. H. Park, M. L. Cho and S. K. Kwok, *Front. Immunol.*, 2021, **12**, 696074.
23. S. H. Yoon, S. M. Ha, S. Kwon, J. Lim, Y. Kim, H. Seo and J. Chun, *Int. J. Syst. Evol. Microbiol.*, 2017, **67**, 1613-1617.
24. J. Chong, P. Liu, G. Zhou and J. Xia, *Nat. Protoc.*, 2020, **15**, 799-821.
25. A. Dhariwal, J. Chong, S. Habib, I. L. King, L. B. Agellon and J. Xia, *Nucleic Acids Res.*, 2017, **45**, W180-W188.
26. N. Segata, J. Izard, L. Waldron, D. Gevers, L. Miropolsky, W. S. Garrett and C. Huttenhower, *Genome Biol.*, 2011, **12**, R60.
27. Infrared Spectroscopy Absorption Table, https://chem.libretexts.org/Ancillary_Materials/Reference/Reference_Tables/Spectroscopic_Parameters/Infrared_Spectroscopy_Absorption_Table, (accessed 11 May, 2022).
28. L. Daasch and D. Smith, *Anal. Chem.*, 1951, **23**, 853-868.

View Article Online
DOI: 10.1039/D2BM01428A
Journal Name ARTICLE

29. A. M. Young, *Biomaterials*, 2002, **23**, 3289-3295.
30. A. Wiegand, W. Buchalla and T. Attin, *Dent. Mater.*, 2007, **23**, 343-362.
31. J. W. Nicholson, N. J. Coleman and S. K. Sidhu, *J. Mater. Sci. Mater. Med.*, 2021, **32**, 30.
32. M. J. Lee, J. S. Kwon, J. Y. Kim, J. H. Ryu, J. Y. Seo, S. Jang, K. M. Kim, C. J. Hwang and S. H. Choi, *Dent. Mater.*, 2019, **35**, 1331-1341.
33. L. Song, Q. Ye, X. Ge, A. Misra, C. Tamerler and P. Spencer, *Dent. Mater.*, 2017, **33**, 564-574.
34. K. Janebodin, Y. Zeng, W. Buranaphatthana, N. Ieronimakis and M. Reyes, *J. Dent. Res.*, 2013, **92**, 524-531.
35. A. P. D. Ribeiro, N. T. Sacono, D. G. Soares, E. A. F. Bordini, C. A. De Souza Costa and J. Hebling, *Clin. Oral Investig.*, 2020, **24**, 1739-1748.
36. C. S. Kovacs, C. Chaussain, P. Osdoby, M. L. Brandi, B. Clarke and R. V. Thakker, *Nat. Rev. Endocrinol.*, 2021, **17**, 336-349.
37. R. Yamamoto, S. Oida and Y. Yamakoshi, *J. Dent. Res.*, 2015, **94**, 1120-1127.
38. X. Wei, J. Ling, L. Wu, L. Liu and Y. Xiao, *J. Endod.*, 2007, **33**, 703-708.
39. M. Alksne, E. Simoliunas, M. Kalvaityte, E. Skliutas, I. Rinkunaite, I. Gendviliene, D. Baltriukiene, V. Rutkunas and V. Bukelskiene, *J. Biomed. Mater. Res. A*, 2019, **107**, 174-186.
40. E. A. Bortoluzzi, L.-N. Niu, C. D. Palani, A. R. El-Awady, B. D. Hammond, D.-D. Pei, F.-C. Tian, C. W. Cutler, D. H. Pashley and F. R. Tay, *Dent. Mater.*, 2015, **31**, 1510-1522.
41. J. S. Kwon, M. J. Lee, J. Y. Kim, D. Kim, J. H. Ryu, S. Jang, K. M. Kim, C. J. Hwang and S. H. Choi, *Sci. Rep.*, 2019, **9**, 1432.
42. X. Li, L. Shang, B. W. Brandt, M. J. Buijs, S. Roffel, C. Van Loveren, W. Crielaard, S. Gibbs and D. M. Deng, *NPJ Biofilms Microbiomes*, 2021, **7**.
43. A. A. Balhaddad, I. M. Garcia, L. Mokeem, M. S. Ibrahim, F. M. Collares, M. D. Weir, H. H. K. Xu and M. A. S. Melo, *J. Dent. Res.*, 2021, DOI: 10.1177/00220345211018189, 220345211018189.
44. P. Zhou, D. Manoil, G. N. Belibasakis and G. A. Kotsakis, *Front. Oral Health*, 2021, **2**, 774115.